Radiative decays of the ψ(3684) into high-mass states

W. Tanenbaum, M. S. Alam, A. M. Boyarski, M. Breidenbach, G. J. Feldman, G. Hanson, J. A. Jaros,
R. R. Larsen, D. Lüke, V. Lüth, H. L. Lynch,* J. M. Paterson, M. L. Perl, I. Peruzzi,† M. Piccolo,† T. P. Pun,
P. Rapidis, B. Richter, R. H. Schindler, R. F. Schwitters, J. Siegrist, and F. Vannucci‡

Stanford Linear Accelerator Center, Stanford University, Stanford, California 94305

G. H. Trilling, J. S. Whitaker,‡ G. S. Abrams, W. Chinowksy, R. G. DeVoe, C. E. Friedberg,§ G. Goldhaber,
A. D. Johnson, J. A. Kadyk, R. J. Madaras, H. K. Nguyen,ǁ F. M. Pierre,¶ B. Sadoulet, and J. E. Wiss

Lawrence Berkeley Laboratory and Department of Physics, University of California, Berkeley, California 94720

(Received 3 August 1977)

Results of studies of radiative decays of the ψ(3684) using the SLAC-LBL magnetic detector at the electron storage ring SPEAR are presented. There are three high-mass states produced in ψ(3684) radiative decays, with masses of 3414 ± 3, 3503 ± 4, and 3551 ± 4 MeV where the errors given do not include an overall mass-scale uncertainty of ± 4 MeV. There is some evidence for a fourth such state at either 3455 or 3340 MeV. The branching ratio for ψ(3684) radiative decay into the state at 3414 MeV is found to be $(7.5 \pm 2.6)\%$. The decay modes of these states into hadrons and into γψ(3095) are studied, yielding information about the branching ratios, spins, and parities of the states. The results are interpreted in the charmonium picture of the high-mass states.

I. INTRODUCTION

The remarkably narrow widths of the ψ(3095) and ψ(3684), hereafter denoted by ψ and ψ′, respectively, are usually interpreted by considering the ψ and ψ′ as bound states of a charmed-quark-antiquark pair, or "charmonium."[1-4] The ψ, being a vector particle, is commonly interpreted as the $^3S_1$ ground state,[5] while the ψ′ is the first radial excitation of the $^3S_1$ state.[6] In this picture, there should be other narrow states of charmonium with masses roughly comparable to the ψ and ψ′ masses. Those charmonium states χ that can be reached by the radiative transitions $\psi' \to \chi\gamma$ or $\psi \to \chi\gamma$ are particularly experimentally accessible. Such states must have the following properties:

1. They must be even under charge conjugation. Hence, they cannot be produced directly by e^+e^- colliding beams through a single virtual photon.

2. They must be less massive than the ψ′.

3. They should be narrow, since their hadronic decays will be suppressed by the Okubo-Zweig-Iizuka (OZI) rule.

4. They must have isospin zero and even G parity. Hence, they may decay hadronically into even numbers of pions.

5. If they are more massive than the ψ, they may in turn decay by the radiative transition χ → ψγ.

6. The ^1S, ^3P, ^1D, etc., states of charmonium are even under charge conjugation. The $^1S_0$ state is a pseudoscalar and most models predict the pseudoscalar masses to lie somewhat below those of the corresponding $^3S_1$ (ψ) states. The lowest-lying $^3P_0$, $^3P_1$, and $^3P_2$ states, with spin-parities 0^+, 1^+, and 2^+, respectively, are usually predicted to lie in mass between the ψ and ψ′. The lowest-lying $^1D_2$, with spin-parity 2^-, may also lie below the ψ′.

The first evidence for such a state was obtained by the DASP collaboration study of the $\psi' \to \psi\gamma\gamma$ decay process.[7] Subsequently, more detailed information on this and other states has been obtained by other groups from the study of hadronic decay modes[8] and γψ decay modes,[9-11] and from observation of monochromatic photons in inclusive photon spectra.[10,12] Altogether, there is evidence for five states. Three states, with masses of about 3415, 3505, and 3550 MeV have been seen in ψ′ radiative decay by at least two independent experiments using different methods.[7-12] A fourth state at 3455 MeV has been seen by us in ψ′ radiative decay through its γψ decay mode.[10] In addition, a state at 2830 MeV has been seen by the DASP collaboration in ψ radiative decay through its decay into two photons.[13] In this paper, we provide an analysis of all the relevant data from the SLAC-LBL magnetic detector at SPEAR, determine our best experimental values for the properties of χ states, and interpret the results in terms of the charmonium picture.[14]

II. THE MAGNETIC DETECTOR

The general features of the magnetic detector have been described in an earlier publication[15]; here we give a brief recapitulation with emphasis on aspects that are of particular importance to the study of radiative decays.
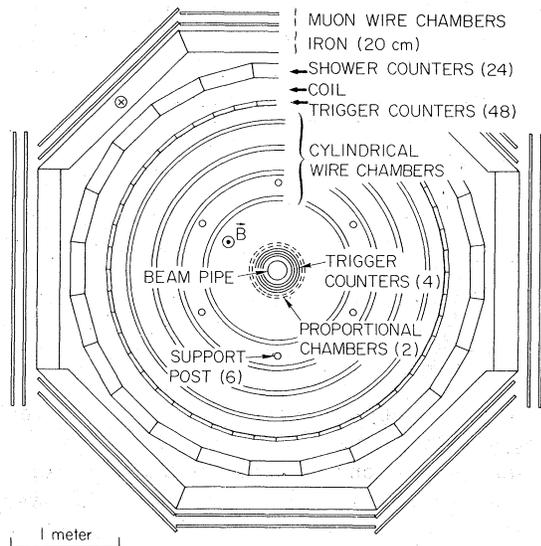
FIG. 1. An end view of the magnetic detector. The iron flux return and muon chambers were removed from the two side sections for much of the running.

Figure 1 shows a sectioned view of the magnetic detector. A particle emanating from the interaction region traverses in sequence:

The vacuum chamber—a corrugated cylinder of 0.15-mm-thick stainless steel at 0.08 ± 0.004 m from the beam line. The chamber has a mean thickness, including the effect of the corrugation, of 0.152 g/cm^2, or 0.011 radiation lengths.

The pipe counters—two cylindrical plastic scintillation counters, at 0.11 and 0.13 m from the beam line and extending ± 0.18 m along the beam line from the center of the interaction region. Each counter has a thickness of 0.70 g/cm^2 or 0.016 radiation lengths.

The proportional chambers—two cylindrical proportional wire chambers, each 0.0043 radiation lengths thick.[16] The inner chamber, at a radius of 0.17 m, has 2.1-mm wire spacing and extends ± 0.254 m along the beam line; the outer chamber, at 0.23-m radius, has 2.8-mm wire spacing and extends ± 0.406 m.

The spark chambers—four double-gap cylindrical wire spark chambers with magnetostrictive readout, each with one gap with $\pm 2°$ stereo angle and one gap with $\pm 4°$ stereo angle.

The trigger counters—48 2.5-cm-thick plastic scintillation counters at 1.5-m radius, each 0.20 m wide and extending ± 1.3 m along the beam line. These counters measure the flight time for particles from the interaction region with an rms resolution of 0.4 nsec.

The solenoid—a 1-radiation-length-thick aluminum coil, coaxial with the beams at 1.7-m radius,

providing an axial magnetic field of 4 kG.

The shower counters—24 counters, each consisting of five 0.64-cm-thick (~1 radiation length) lead sheets each followed by a 0.64-cm-sheet of Pilot F plastic scintillator. The counters are 0.46 m wide and have active length of 3.1 m.

The hadron filter—0.2 m of iron plates outside the shower counters, serving also as a flux return for the magnetic field.

Muon chambers—planar wire spark chambers, covering about 70% of the aziumth, for detecting particles penetrating the hadron filter.

The trigger for the magnetic detector requires, coincident with the beam collision, signals in both pipe counters and two or more coincidences of trigger counters with their backing shower counters. This essentially requires two or more charged particles with momenta $\gtrsim 200$ MeV/c to trigger the detector. Charged particles are tracked by the two proportional chambers and the four double-gap spark chambers, which cover the full azimuth and the polar angle θ from 50° to 130°. Particles must traverse at least the inner two spark chambers in order to be tracked; this implies a minimum transverse momentum of 55 MeV/c. When the beam position is included as a point on the track, the charged-particle rms momentum resolution is $\Delta p/p = 0.015\, p$, where p is expressed in GeV/c. There is an additional contribution due to multiple scattering of $\Delta p/p = 0.006$, which must be added in quadrature. For charged tracks which do not originate from the beam, such as electrons or positrons from a photon conversion, the resolution is about a factor of 2 poorer above 110 MeV/c. Below 110 MeV/c, the resolution without the beam position deteriorates rapidly, since the track no longer traverses all the chambers.

III. IDENTIFICATION OF χ STATES

The data sample used in this paper consists of ~330 000 events recorded with a c.m. energy set at the ψ' mass and ~150 000 events recorded at the ψ mass. A valid event meets the above trigger requirements, and in addition contains two or more reconstructed charged tracks that originate near the point where the beams collide. From this data sample, we search for the existence of charmonium states by three different methods described respectively in parts A, B, and C of this section.

A. Inclusive photon spectra

By searching for structure in the inclusive photon spectra from ψ and ψ' decay we observe radiative decays to even-charge-conjugation states in-

dependently of the decay modes of such states. Such observations enable us to measure the total branching fraction for a radiative decay. Since a large fraction of ψ' decays include a ψ,[17] it is necessary to study the inclusive spectra of both ψ and ψ' to associate any structure in the spectra with the correct parent. Results of such an analysis have been published previously.[10]

1. Photon detection

Photons are detected by their conversion to electron-positron pairs in material near the beam line. The material effective as a converter is sketched in Fig. 2; it includes the vacuum pipe, the pipe counters, and the proportional wire chambers, a total of 0.052 radiation lengths of material located 8 to 22 cm from the beam line. The conversion probability for photons at normal incidence is 0.030 at $E_\gamma = 0.2$ GeV and rises to 0.039 at 2 GeV.

The electron and positron from a conversion are detected by the cylindrical spark chambers and the two proportional chambers. A minimum transverse momentum of ~55 MeV/c is required for a charged particle originating near the beam line to traverse two or more spark chambers. A study of the angular distribution of detected charged particles relative to the beam has shown that tracks are found with high efficiency for $|\cos\theta| < 0.6$. The transverse-momentum requirement for each particle and the detector angular acceptance determine the efficiency for detecting converted pairs.

Figure 3 shows the calculated photon-detection efficiency with the cuts $|\cos\theta| < 0.6$ and transverse momentum of both the electron and the positron > 0.055 GeV/c. The calculation takes into account the energy-dependent conversion probability and the detector acceptance, including the
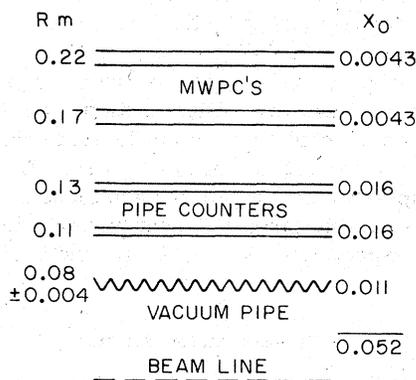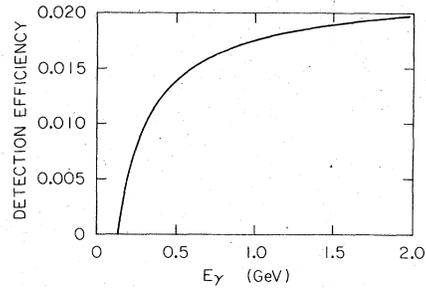

FIG. 3. Photon-detection efficiency versus photon energy.

15% loss of acceptance within $|\cos\theta_\gamma| < 0.6$ due to the spark-chamber support posts. The photon angular distribution is assumed to be isotropic; the acceptance for a $1 + \cos^2\theta$ distribution is lower by 16%.

To identify pairs of oppositely charged particles with measured opening angle α as electron-positron pairs, we calculate the invariant mass-squared $M^2 = 2P_+ P_- (1 - \cos\alpha) \approx P_+ P_- \alpha^2$ and select those with small M^2 as photon conversions. Accurate calculation of α at the conversion point is complicated by the uncertainty as to where in the absorber in Fig. 2 the conversion occurred. This uncertainty introduces an error of at most 0.0006 (GeV/c^2)^2 into the determination of M^2. Consequently a cut $M^2 < 0.000\,75$ GeV^2 was imposed to select conversion pairs. This cut keeps essentially all the externally converted pairs, and admits ~20% accidental-hadron-pair background as estimated from the like-charged pairs. Approximately 34% of the internal conversions will fall within this cut, constituting ~7% of the total pairs selected.

2. Photon energy resolution

The photon energy is calculated as the sum of the energies of the positron and electron. The photon energy resolution is determined by the momentum resolution of the tracking chambers, including the contribution from multiple scattering, and by the uncertainty in the energy loss of the electron and positron by ionization or radiation as they pass through the material between the conversion point and the chamber. The solid line in Fig. 4 shows the mean rms momentum resolution contribution to photon energy resolution calculated by combining in quadrature the estimated momentum errors of the two tracks of a conversion pair. The rise at low energy is due to the poor momentum resolution of tracks which traverse fewer than the full complement of tracking chambers.

The overall photon energy resolution will be the combination of all these effects. The dashed line

R m X_0

0.22 ══════════════════ 0.0043
                    MWPC'S
0.17 ══════════════════ 0.0043

0.13 ══════════════════ 0.016
                PIPE COUNTERS
0.11 ══════════════════ 0.016

0.08
±0.004 ∿∿∿∿∿∿∿∿∿∿ 0.011
               VACUUM PIPE

                                    0.052
              BEAM LINE ─ ─ ─

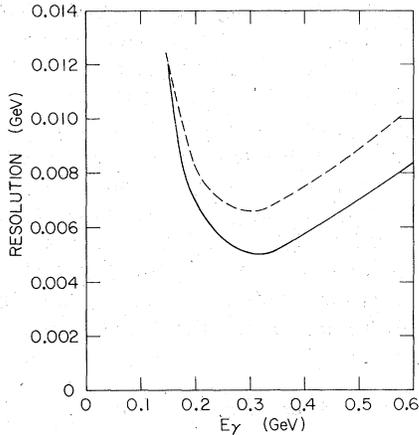FIG. 2. The effective converter, with thickness and distance from the beam line.

FIG. 4. Photon rms energy resolution versus photon energy. The solid line indicates the effect of the momentum resolution of charged particles. The dashed line includes also the effect of energy loss by ionization and radiation.

in Fig. 4 is the sum in quadrature of the momentum resolution, ionization loss, and the errors introduced by radiative effects. The rms photon resolution is 2–4% for photon energies from 0.2 to 2 GeV.

3. The inclusive photon spectra

Figure 5(a) is the inclusive spectrum for 4659 photons from 150 000 ψ decays. The data are plotted in 4% energy bins, and no correction has been made for energy loss in the converter. These spectra have a gross shape determined by the acceptance folded into the photon spectrum from hadron decays, predominantly π^0 decay products. The photon spectrum from π^0 decay has its maximum at $E_\gamma = m_{\pi^0}/2 = 67$ MeV and falls roughly exponentially; the observed spectrum, zero below 110 MeV and with a broad maximum from ~250–500 MeV, indicates the effect of increasing acceptance multiplying the falling produced photon spectrum. The smooth curve in Fig. 5(a) is the inclusive photon spectrum from an all-pion-phase-space Monte Carlo simulation of ψ decays, normalized to the data in the 300–350-MeV region. The shape of the experimental spectrum agrees rather well with the Monte Carlo results except in the low-energy region where the acceptance varies rapidly.

Figure 5(b) shows the corresponding inclusive spectrum for 14 000 photons from 330 000 ψ' decays, again presented in 4% energy bins. The general shape of this spectrum is very similar to that of the ψ. This is not surprising since 57% of ψ' decays contain a ψ.[17] In addition, there is a clear peak at $E_\gamma \sim 260$ MeV with a full width at

half-maximum of ~20 MeV, consistent with the expected resolution of a narrow signal. To check that this peak is not the result of the rapidly varying acceptance, the data were analyzed imposing successively cuts of 55, 65, and 75 MeV/c on the transverse momenta of the electron and positron. The 55-MeV/c cut corresponds to the physical limits of the detector; the 65-MeV/c and 75-MeV/c cuts reduce the acceptance by 16% and 31%, respectively, and change the slope of the acceptance in the 260-MeV region dramatically. Figures 6(a), 6(b), 6(c) show the ψ' inclusive photon spectrum with 55-MeV/c, 65-MeV/c, and 75-MeV/c transverse-momentum cuts. To the extent that the peak remains visible it stays at the same energy with approximately the same observed width, and therefore is not being shaped by the acceptance.

After correction for the ionization losses of the electron and positron, the peak is at 261 ± 10 MeV. This corresponds to a transition from ψ' to a state of mass 3413 ± 11 MeV. We will hereafter call this state $\chi(3415)$. As will be seen in Sec. III C, a strong signal at the same mass is observed in the study of hadronic decay modes of χ states. There is no other likely explanation of
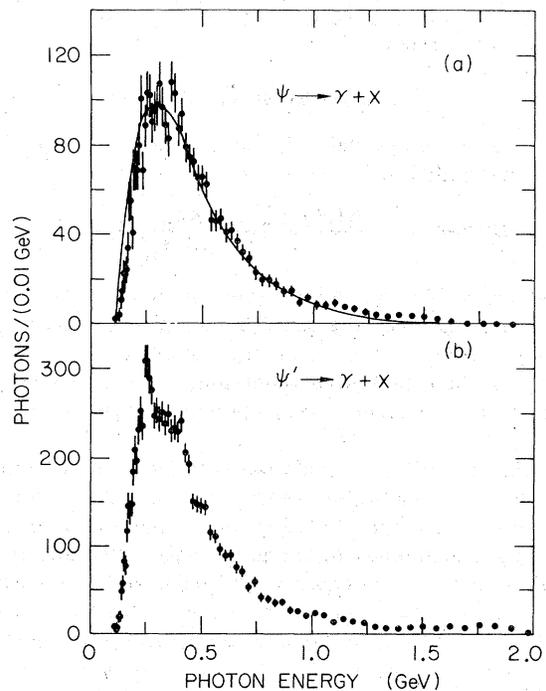

FIG. 5. (a) The inclusive photon spectrum from ψ. The solid line is the spectrum from a Monte Carlo simulation of ψ events. (b) The inclusive photon spectrum from ψ'.

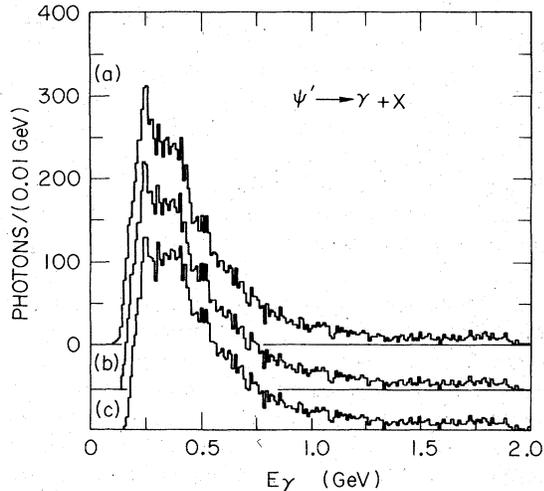FIG. 6. The ψ' photon spectrum with charged-particle transverse-momentum cuts: (a) 55 MeV/c, (b) 65 MeV/c, and (c) 75 MeV/c.

this bump. The photons from $\eta \rightarrow \gamma\gamma$ from inclusive η production will peak at $m_\eta/2 = 275$ MeV and will have a broad spectrum reflecting the η momentum distribution. The photons from $\psi' \rightarrow \psi\eta$, $\eta \rightarrow \gamma\gamma$ will be Doppler-broadened and spread uniformly from 193 to 389 MeV. The absence of the peak in the ψ photon spectrum rules out the possibility that it originates from ψ decays from the $\psi' \rightarrow \psi$ cascade events.

4. Branching-ratio calculation

The branching ratio of the transition $\psi' \rightarrow \gamma\chi(3415)$ is calculated as

$$B(\psi' \rightarrow \gamma\chi) = \frac{N(\psi' \rightarrow \gamma\chi)/(\epsilon_\gamma \times \epsilon_R \times \epsilon_{tr}^s)}{N(\psi' \rightarrow \text{all})/\epsilon_{tr}^{all}}, \quad (1)$$

where $N(\psi' \rightarrow \gamma\chi)$ is the excess number of events in the peak over the smooth background, and $N(\psi' \rightarrow \text{all})$ is the total number of ψ' events used to compile the inclusive spectrum, with the contributions from nonresonant hadronic and QED events removed.

The quantity ϵ_R, calculated to be ~ 0.8, is a correction for radiative losses, ϵ_{tr}^{all} is the average trigger efficiency for all events, and ϵ_{tr}^s is the trigger efficiency for signal events. The efficiency ϵ_{tr}^s is taken to be equal to ϵ_{tr}^{all} enhanced by the contribution from the converted photon—this assumes that the χ(3415) has multibody decays similar to ψ or ψ'. The ratio $\epsilon_{tr}^{all}/\epsilon_{tr}^s$, determined by counting the fraction of events in which a photon conversion track was an essential part of the trigger, is 0.74 ± 0.07. There is a further 7% correction to the branching ratio to account for internal con-

versions. The branching ratio is 0.063 ± 0.022 for an isotropic photon distribution and 0.075 ± 0.026 for a $(1 + \cos^2\theta)$ distribution (favored by the data in Sec. IIIC). The 35% relative error is the sum in quadrature of the 17% statistical error and estimated systematic errors of 20% in background subtraction, 20% in the photon detection efficiency, 10% in the $\epsilon_{tr}^{all}/\epsilon_{tr}^s$ calculation, and 5% in the radiative correction. This result is in good agreement with the results of the SPEAR SP-27 collaboration[12] and slightly larger than the upper limits found by the HEPL experiment at SPEAR.[18]

5. Branching-ratio limits

We see no clear monochromatic signals in the ψ or ψ' spectra other than the line for the $\psi' \rightarrow \gamma\chi$(3415) decay. To calculate the upper limits for branching ratios for monochromatic signals, we replace the number of signal events in the branching-ratio calculation by the excess over the smooth background plus twice the error on total number within a FWHM (full width at half-maximum) photon energy resolution. Allowing for the $\sim 30\%$ estimated errors, we interpret these limits as 90% confidence-level upper limits. Table I gives these upper limits for representative photon energies above 250 MeV at ψ and ψ'. The upper limits on the branching ratios for $\psi \rightarrow \gamma X$(2830) and $\psi' \rightarrow \gamma X$(2830) are 3.9% and 1%, respectively, where the X(2830) is the state at 2830 ± 30 MeV reported by the DASP collaboration in ψ radiative decay.[13]

Below 250 MeV, the small and rapidly varying photon-detection efficiency and the poorer photon energy resolution make recognition of a monochromatic signal difficult. Unfortunately, the photons from transitions of ψ' to χ(3550), χ(3505), and the possible state at 3455 MeV (see Secs. IIIB and IIIC) are below this threshold and are not accessible to study by this method.

TABLE I. 90%-confidence-level branching-ratio limits for monochromatic photon production above 0.250 GeV at ψ and ψ'.

ψ(3095)		ψ'(3684)	
E_γ (GeV)	Limit	E_γ (GeV)	Limit
0.26	0.039	0.40	0.028 [a]
0.37	0.038	0.50	0.022
0.51	0.024	0.74	0.011
0.80	0.014	1.05	0.010
1.10	0.008		

[a] Limit for a narrow peak. See text for a discussion of complications due to the cascade photons.

The Doppler-shifted photons from $\chi \rightarrow \gamma\psi$ decays are more than doubled in expected width, and therefore are difficult to separate from the background and from each other. Thus, our monochromatic limits do not apply to $\chi \rightarrow \gamma\psi$ decays. Furthermore, the presence of the Doppler-broadened second photons from the decays of the known χ states makes the background beneath any signal in the 350–450-MeV region difficult to estimate.

B. $\psi' \rightarrow \gamma\gamma\psi$

1. Identification of cascade processes

Charmonium states of even charge conjugation intermediate in mass between ψ and ψ' may be produced in radiative decays of ψ' and may subsequently decay radiatively to ψ, as shown in the following sequence:

$$\psi' \rightarrow \gamma\chi \qquad\qquad (2)$$
$$\searrow\gamma\psi .$$

In the simple charmonium model, in fact, the $^3P_{0,1,2}$ states are expected to decay dominantly to $\gamma\psi$.[3–4] Thus, peaks in the $\psi\gamma$ mass distribution from $\psi' \rightarrow \gamma\gamma\psi$ decays may reveal the presence of such states. Earlier results of such an analysis have been published.[9–10]

The $\psi' \rightarrow \gamma\gamma\psi$ events can be identified if one of the photons converts into an e^+e^- pair and the ψ decays by its e^+e^- or $\mu^+\mu^-$ mode. Photon conversions are selected by almost the same criteria as in Sec. III A.[19] Background from $\psi' \rightarrow \pi^+\pi^-\psi$ events where the $\pi^+\pi^-$ simulate a converted photon is negligible, since the $\pi^+\pi^-$ mass spectrum peaks strongly at large values.[20] The ψ is identified by its lepton pair decay; the observed lepton pair mass is required to lie between 2.97 and 3.22 GeV and is then constrained to the ψ mass. Two cuts are applied to reduce the background from $\psi' \rightarrow e^+e^-$ or the QED process $e^+e^- \rightarrow e^+e^-$ where one of the electrons radiates a photon: First, electron-pair events are rejected

when the angle between the energetic electron and positron is greater than 177.5°, eliminating more than 95% of the radiative background, but only ~8% of real $\psi' \rightarrow \gamma\gamma\psi$, $\psi \rightarrow e^+e^-$ events; second, events are rejected if the converted photon is collinear within 10° with one of the leptons—five events are rejected with this cut.

Figure 7 shows the missing mass squared, m_x^2, recoiling against the $\psi\gamma$ system for the 54 events surviving the selection cuts. There is a peak at zero m_x^2 corresponding to true $\psi' \rightarrow \gamma\gamma\psi$ events and a broad background from $\psi' \rightarrow \pi^0\pi^0\psi$ where one photon from a π^0 converted. Under the hypothesis of $\psi' \rightarrow \gamma\gamma\psi$, the direction of the missing photon may be predicted from the observed photon and the ψ. The unconverted photon may be detected in the 24 shower counters, which cover 65% of the solid angle and have resolution of ~10° in azimuthal angle. The shading in Fig. 7 flags the detection of such additional photons in the shower counters: Darkly shaded events have a shower-counter signal consistent with the missing photon direction assuming a $\gamma\gamma\psi$ decay, lightly shaded events have no unconverted photons detected, and unshaded events have one or more photons detected in counters inconsistent with the $\psi\gamma\gamma$ hypothesis (as expected for $\psi' \rightarrow \pi^0\pi^0\psi$ events). The high correlation of shading with small m_x^2 corroborates the identification of events with small m_x^2 as $\psi' \rightarrow \gamma\gamma\psi$ events.

The 27 shaded events with -0.03 $(\text{GeV}/c^2)^2$ $< m_x^2 < 0.03$ $(\text{GeV}/c^2)^2$ are kept as $\gamma\gamma\psi$ candidates. The unconverted photon is detected in the shower counters in 15 of these events, consistent with the shower counter acceptance and efficiency. Figure 8 shows the missing mass squared M_x^2 recoiling against the ψ for these 27 events and also for events with three or four detected charged tracks in which a muon pair from ψ decay was detected— dominantly $\psi' \rightarrow \pi^+\pi^-\psi$. The M_x^2 distribution for the three- and four-track events peaks at high values; the same is expected for $\psi' \rightarrow \pi^0\pi^0\psi$ events. In contrast, the 27 candidates for $\psi' \rightarrow \gamma\gamma\psi$ have a roughly flat M_x^2 distribution, as expected for radiative cascades by sequence (2).[21] Six events with $M_x^2 > 0.27$ $(\text{GeV}/c^2)^2$ are removed as possible $\psi' \rightarrow \psi\eta$, $\eta \rightarrow \gamma\gamma$ events (four such events are expected).

The remaining 21 events are constrained to fit the reaction $\psi' \rightarrow \gamma\gamma\psi$. There are two $\psi\gamma$ combinations for each event; their effective masses are plotted against one another in Fig. 9. The shaded events have the unconverted photon detected in the proper shower counter. The expected background is one unshaded event and $\frac{1}{4}$ shaded event.

There are three main clusters of events. The mass spread of the high-mass projection of each of these clusters is consistent with the expected
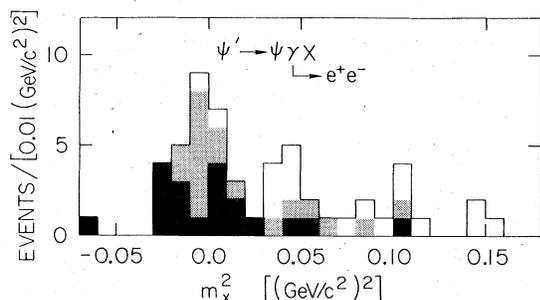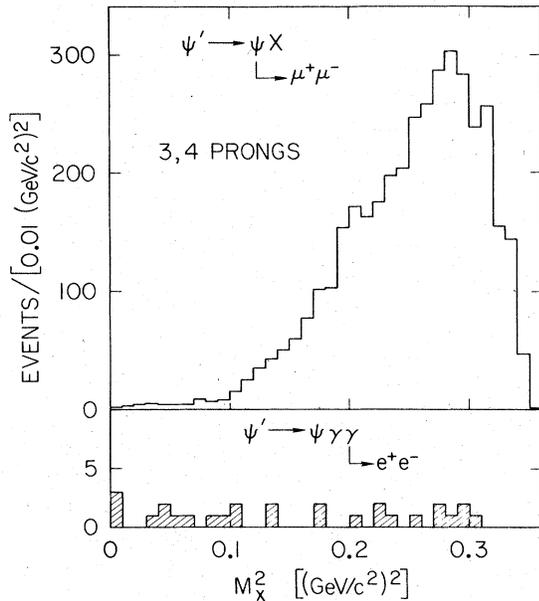

FIG. 7. The missing mass squared recoiling against $\psi\gamma$ in $\psi\gamma\gamma$ candidates with one photon converted. The shading is discussed in the text.

FIG. 8. Missing mass squared recoiling against the ψ for the 27 $\psi\gamma\gamma$ events and also for all 3- and 4-prong events in which a ψ was detected.

rms resolution of ~8 MeV. The masses of the three corresponding states are 3543 ± 7 MeV, 3504 ± 5 MeV, and 3454 ± 7 MeV which we will hereafter call $\chi(3550)$, $\chi(3505)$, and $\chi(3455)$, respectively. As usual, we take $M(\psi') = 3684$ MeV. The mass spread of the low-mass projections of
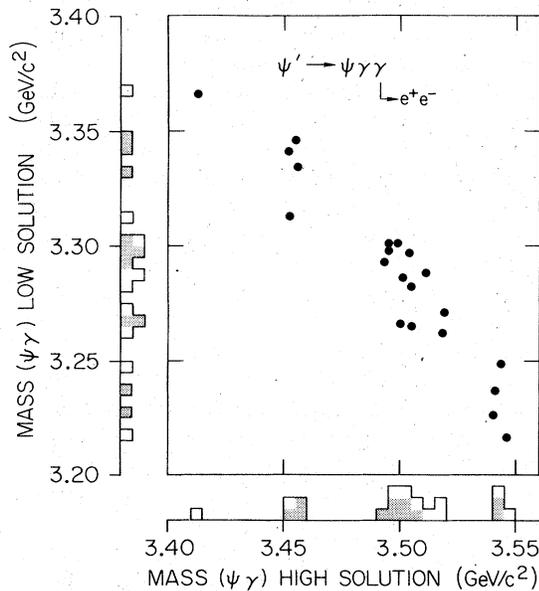

FIG. 9. The two solutions for $\psi\gamma$ masses from 21 $\psi\gamma\gamma$ events.

each of the clusters is consistent with the expected Doppler-broadened resolution of ~14 MeV, and inconsistent with a resolution of 8 MeV, with a confidence level of less than 0.025 for each cluster. However, the events at 3454 MeV can be explained by a state at 3340 MeV with three events and one event background. The states $\chi(3550)$ and $\chi(3505)$ can be identified with states observed through hadronic decays; there is no evidence in hadronic channels for a state at 3455 MeV or 3340 MeV (see Sec. III C). The single event at 3413 MeV is either from the $\chi(3415)$ or a background event.

2. Branching-ratio determination

Correcting for ψ branching ratios and the photon-detection efficiency, we can calculate branching-ratio products for $\psi' \to \gamma\chi$, $\chi \to \gamma\psi$. We define the branching-ratio product as follows:

$$B(\psi' \to \gamma\psi, \ \chi \to \gamma\psi) = B(\psi' \to \gamma\psi)B(\chi \to \gamma\psi). \quad (3)$$

The branching-ratio products for $\psi' \to \gamma\chi$, $\chi \to \gamma\psi$ are $(0.8 \pm 0.4)\%$, $(2.4 \pm 0.8)\%$, and $(1.0 \pm 0.6)\%$ for $\chi(3455)$, $\chi(3505)$, and $\chi(3550)$, respectively— all four events have been counted in the $\chi(3455)$. Taking the event at 3413 MeV in the high-mass projection as signal, the branching-ratio product for $\chi(3415)$ is $(0.2 \pm 0.2)\%$. The branching-ratio products obtained by the SP-27 collaboration are an order of magnitude higher than our result for the $\chi(3415)$ and a factor of 2 higher for the $\chi(3505)$ and the $\chi(3550)$.[12] The differences are at the level of 1.8, 1.5, and 1.0 standard deviations, respectively.

C. Hadronic decay modes of χ

1. General procedure

The χ states can be identified and some of their hadronic decay modes can be studied by analysis of the processes

$$\psi' \to \chi\gamma, \quad (4a)$$

$$\chi \to \text{charged hadrons}. \quad (4b)$$

In the above chain, the photon is not directly detected, but its presence can be inferred from measurements of missing energy and missing momentum provided that all the hadrons from the χ decay are detected. The specific decay modes studied are the following:

$$\chi \to \pi^+\pi^-\pi^+\pi^- \quad (5a)$$

$$\to \pi^+\pi^-K^+K^- \quad (5b)$$

$$\to \pi^+\pi^-p\bar{p} \quad (5c)$$

$$\to \pi^+\pi^-\pi^+\pi^-\pi^+\pi^- \quad (5d)$$

$$\to \pi^+\pi^- \quad (5e)$$

$$\to K^+K^-. \quad (5f)$$

Since the efficiency for detecting all outgoing charged hadrons is rather high in comparison to the efficiency of detecting photons in the manner described in Sec. III A, this procedure potentially has a high sensitivity for observing χ states. It suffers, however, from backgrounds produced by the following two types of reactions:

$$\psi' \rightarrow (\text{charged hadrons}) + \pi^0 \tag{6}$$

and

$$\psi' \rightarrow \text{charged particles}. \tag{7}$$

In reaction (6), the "photon" is actually a π^0 produced with a collection of charged hadrons. In reaction (7), there is no missing neutral particle; but, because of finite measurement errors, the observations are consistent with the emission of a low-energy photon.

The background from decay processes (6) can fortunately be kept quite small for the following reasons:

(a) Decay modes of this form have relatively small branching ratios.

(b) Such decay modes have a π^0 spectrum spread over a wide range of energies, whereas the photons in (4a) are monoenergetic and have relatively small energy.

(c) The measurement of neutral missing mass by which one distinguishes a photon from a pion is most precise when the energy taken up by the neutral system is small; this is just the situation applicable for reaction (5a).

These points have already been discussed in some detail in an earlier paper,[8] and the more extensive data sample now available confirms the validity of the γ-π^0 separation.

Processes (7) can usefully be subdivided into the following mutually exclusive groups:

$$\psi' \rightarrow \pi^+ \pi^- \psi, \quad \psi \rightarrow \text{charged particles}, \tag{8a}$$

$$\psi' \rightarrow e^+ e^-, \mu^+ \mu^-, \tag{8b}$$

$$\psi' \rightarrow \text{charged hadrons}. \tag{8c}$$

As will be seen in more detail below, the large background from (8a) and (8b) can be completely removed by appropriate cuts. Branching ratios for processes (8c) are relatively small, and their presence does not significantly affect the study of the states discussed in this paper whose mass is at least 130 MeV below the ψ mass. However, they do tend to mask any radiative decay mode leading to photons of energy less than 80 MeV especially since the branching ratio for such states may be expected to be small. Since the pseudoscalar states might be expected to have masses just slightly below those of the corresponding vector (ψ) states, this background will seriously limit

the sensitivity of any search for such states if indeed they lie in that mass region.

The decay modes (5b), (5c), and (5f) involve charged particles other than pions. From the point of view of kinematics, processes such as $\psi' \rightarrow \gamma \chi \rightarrow \gamma \pi^+ \pi^- K^+ K^-$ or $\gamma \pi^+ \pi^- p\bar{p}$ can be ambiguous with $\psi' \rightarrow \pi^+ \pi^- \pi^+ \pi^- (n\pi^0)$. To help remove such background, we have used time-of-flight (TOF) information and constructed for each event a measure of goodness of fit as follows:

$$\chi^2_{\text{TOF}} = \sum_{\text{tracks}} \frac{(t_{\text{meas}} - t_{\text{pred}})^2}{\sigma^2},$$

where the sum is taken over all tracks for which time-of-flight information exists, t_{meas} and t_{pred} are the measured and predicted flight times based on the momentum measurements and the assumed identifies of the charged particles. This χ^2_{TOF} was used for both decay modes (5b) and (5c) in a manner described in the next section. For decay mode (5f), the high momenta of the kaons preclude useful separation in this way. However, the multipion background in the kinematic region which simulates (5f) is very small, and the separation between (5e) and (5f) can very adequately be made on the basis of the goodness of the one-constraint (1C) fit.

2. Selection of data samples

We now proceed to a more detailed discussion of the selection of data samples for the various χ decay modes (5).

a. $\pi^+ \pi^- \pi^+ \pi^-$.

(*i*) $|\text{Missing mass}|^2 \leq 0.05$ $(\text{GeV}/c^2)^2$ to eliminate multi-π^0 events.

(*ii*) (Missing energy—missing momentum) ≤ 0.1 GeV/c to avoid confusion with decay modes $\chi \rightarrow \pi^+ \pi^- K^+ K^-$. For such modes, treated as though they consisted of $\pi^+ \pi^- \pi^+ \pi^-$, the missing energy would normally be about 0.2 GeV greater than the missing momentum.

(*iii*) (Missing mass recoiling against any $\pi^+ \pi^-$) ≤ 3.05 GeV/c^2 to remove background from $\pi^+ \pi^- \psi$ and $\eta \psi$ followed by $\psi \rightarrow e^+ e^-$ or $\mu^+ \mu^-$ decays.

b. $\pi^+ \pi^- K^+ K^-$.

(*i*) $|\text{Missing mass}|^2 \leq 0.05$ $(\text{GeV}/c^2)^2$.

(*ii*) (Missing energy (calculated as if all tracks are pions)—missing momentum) > 0.1 GeV/c to avoid confusion with the mode $\chi \rightarrow \pi^+ \pi^- \pi^+ \pi^-$.

(*iii*) Same as (*iii*) for $\pi^+ \pi^- \pi^+ \pi^-$.

(*iv*) $\chi^2_{\text{TOF}}(\pi^+ \pi^- K^+ K^-) < \chi^2_{\text{TOF}}(\pi^+ \pi^- \pi^+ \pi^-)$.

It may be noted that requirements (*ii*) for the above two modes guarantee that there be no overlap between the data samples.

c. $\pi^+ \pi^- p\bar{p}$.

(*i*), (*ii*), (*iii*) Same as for $\pi^+ \pi^- K^+ K^-$.

(iv) χ^2_{TOF} ($\pi^+\pi^-p\bar{p}$) $< \chi^2_{\text{TOF}}(\pi^+\pi^-K^+K^-)$ and $<\chi^2_{\text{TOF}}$ ($\pi^+\pi^-\pi^+\pi^-$).

$d.$ $\pi^+\pi^-\pi^+\pi^-\pi^+\pi^-$.

(i) |Missing mass|$^2 \le 0.05$ (GeV/c^2)^2.

(ii) Same as (ii) for $\pi^+\pi^-\pi^+\pi^-$.

(iii) (Missing mass recoiling against any $\pi^+\pi^-$) outside the range 3.05–3.20 GeV/c^2 to remove $\pi^+\pi^-\psi$ contamination.

The requirement (iii) here is much less restrictive than for the four-body modes for two reasons: There is much less $\pi^+\pi^-\psi$ background to remove, and such removal tends to cut more deeply into the useful data sample.

$e.$ $\pi^+\pi^-$ or K^+K^-.

(i) (Pulse height for both particles in shower counters)< lower limit of range appropriate to electrons.

(ii) Neither particle gives signals in muon chambers within 4 standard deviations of the predicted trajectory.

(iii) Both particle momenta >1000 MeV/c and azimuthal angle between track momentum vectors $>160°$.

(iv) Missing momentum transverse to the average $\pi^+\pi^-$ or K^+K^- line ≥ 50 MeV/c to remove radiative e^+e^- and $\mu^+\mu^-$ decays not already cut out by (i) and (ii).

(v) Effective mass of charged particles when treated as $\pi^+\pi^-$ outside range 3020–3190 MeV to remove residual $\psi \to e^+e^-$, $\mu^+\mu^-$ events found in such decay modes as $\psi' \to \pi^0\pi^0\psi, \eta\psi, \gamma\gamma\psi$.

The major problem in the selection of the sample for $\pi^+\pi^-$ or K^+K^- is obviously the removal of dilepton events arising from either ψ' decay or decay of ψ produced from ψ' in a cascade process. Cuts (i), (ii), (iv), and (v) reduce this background to a negligible level.

3. Analysis of χ hadronic decays

$a.$ *General features.* Samples selected in the manner just described were fit to the 1-constraint hypothesis (4) with the bubble-chamber program SQUAW, and those events giving satisfactory fits were retained in the final data samples. Ambiguities between the $\pi^+\pi^-$ and K^+K^- decay modes were largely resolved by the kinematic fit. The 15% of these events which remained unresolved were apportioned according to which χ^2 value was the smaller (although the difference between the two χ^2 values was of course small). There were no other ambiguities between the various channels (5a)–(5f). The mass resolutions in the regions of interest for χ states are typically ±20 MeV/c^2 after the fit.

The resulting mass spectra for the various channels are shown in Figs. 10 and 11. From these spectra, one can make the following observations:
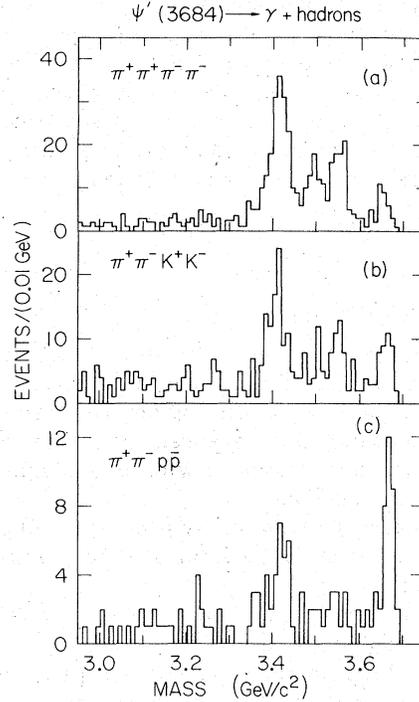

FIG. 10. Mass spectrum for multihadron state X fit to the reaction $\psi' \to \gamma X$ with X being (a) $\pi^+\pi^-\pi^+\pi^-$, (b) $\pi^+\pi^-K^+K^-$, (c) $\pi^+\pi^-p\bar{p}$.

(1) For all channels, the mass region above 3.3 GeV/c^2 is dominated by rather clear structures which will be discussed below. The event populations outside of this region are a rough measure
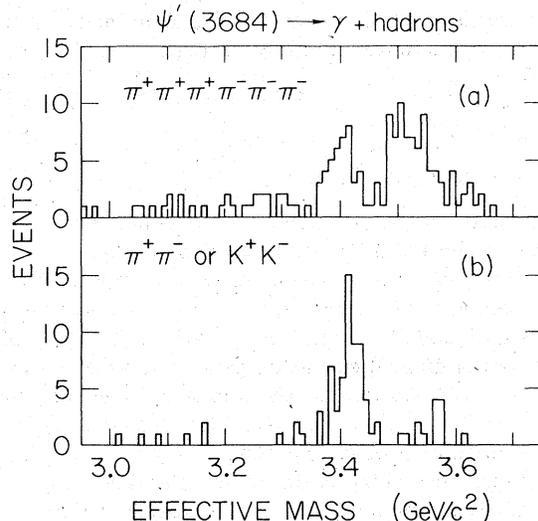

FIG. 11. Mass spectrum for multihadron state X fit to the reaction $\psi' \to \gamma X$ with X being (a) $\pi^+\pi^+\pi^+\pi^-\pi^-\pi^-$, (b) $\pi^+\pi^-$ or K^+K^-.

of the background remaining after the cuts dis-
cussed earlier. The absence of events near 3.7
GeV/c^2 and 3.1 GeV/c^2 in the $\pi^+\pi^-$, K^+K^- spectra
testifies to the successful removal of dilepton
background arising from ψ' or ψ decay.

(2) Every one of the decay channels shows a
prominent peak at around 3415 MeV.

(3) The 4π and $\pi^+\pi^-K^+K^-$ spectra also show peaks
near 3500 and 3550 MeV although the $\pi^+\pi^-K^+K^-$
signal near 3500 MeV is weak. The 6π spectrum
above 3415 MeV is compatible with populations
from these two states, but they are not clearly re-
solved. Compelling support for the interpretation
of the spectra of Figs. 10 and 11 in terms of two
states at 3500 and 3550 MeV comes from the ob-
servations of these two states by the techniques
discussed in Sec. III B.

(4) The summed $\pi^+\pi^-$ and K^+K^- spectra show
fairly clear structure at 3550 MeV, but no signif-
icant population at 3500 MeV.

(5) There is no evidence for hadronic signals at
3455 or 3340 MeV, the possible masses for the
additional state suggested by the cascade data of
Fig. 9.

(6) There are clear peaks at the upper ends of
the $\pi^+\pi^-\pi^+\pi^-$, $\pi^+\pi^-K^+K^-$, and $\pi^+\pi^-p\bar{p}$ spectra. These
correspond to the direct decay modes $\psi'\to\pi^+\pi^-\pi^+\pi^-$,
$\pi^+\pi^-K^+K^-$, $\pi^+\pi^-p\bar{p}$. These peaks appear in the
histograms centered slightly below the ψ' mass of
3684 MeV because the 1C fit to which they are
subjected produces a "photon" of necessarily
positive energy and, hence, shifts them downward
by an amount comparable to the measurement
errors in momentum and energy balance.

(7) There are a few events in the $\pi^+\pi^-\pi^+\pi^-$ and
$\pi^+\pi^-K^+K^-$ spectra between the clear peaks at 3550
MeV and at the upper end of the histograms. These
events may arise from the tails of the peaks, back-
ground, or from the decay of a pseudoscalar state
of mass just below that of the ψ'. There are not
enough data to resolve this question.

The results of perfoming fits to the histograms
in Figs. 10 and 11, as described in the next sec-
tion, and taking appropriately weighted averages
for the various channels leads to the following
masses deduced from hadronic decay modes:

$$M = 3414 \pm 3, \quad 3502 \pm 6, \quad 3555 \pm 5 \text{ MeV}/c^2$$

for the three observed χ states [taking as always
$M(\psi') = 3684$ MeV]. These values are in good
agreement with those deduced earlier from ob-
servations of converted photons, and can be identi-
fied with the $\chi(3415)$, $\chi(3505)$, and $\chi(3550)$, re-
spectively.

b. Branching ratios. The fraction of ψ' decays
which proceed via (4a) with a particular hadronic
final state f provides a measure of the product of
the two branching ratios,

$$B(\psi'\to\gamma\chi, \; \chi\to f) = B(\psi'\to\gamma\chi)B(\chi\to f). \tag{9}$$

To determine the left-hand side of (9), we use the
following relation:

$$B(\psi'\to\gamma\chi, \; \chi\to f) = \frac{N(\psi'\to\gamma\chi, \; \chi\to f)}{N(\psi'\to g)}$$

$$\times \frac{\epsilon(g)}{\epsilon(f)} B(\psi'\to g), \tag{10}$$

where g is a conveniently chosen final state pro-
duced in ψ' decay with known branching ratio
$B(\psi'\to g)$; $\epsilon(f)$, $\epsilon(g)$ are detection efficiencies for
the f and g final states, and $N(\psi'\to\gamma\chi, \; \chi\to f)$,
$N(\psi'\to g)$ are the observed event populations for the
two final states.

Table II shows the ψ' final states g used in (10)
for the branching-ratio normalizations. These
final states are chosen to have just the same num-
bers of prongs as the corresponding χ states with
which they are compared to remove some of the
systematic uncertainties.

To determine the populations of the various χ
states in the several hadronic final states studied,

TABLE II. ψ' decays used in normalization.

ψ' decay mode used	No. of decays	Efficiency	Branching ratio	Corresponding χ final states
$\pi^+\pi^-\psi; \; \psi\to \begin{cases} e^+e^- \\ \mu^+\mu^- \end{cases}$	2660 ± 100	0.22	$(4.6 \pm 0.7)\%$	$\pi^+\pi^-\pi^+\pi^-$ $\pi^+\pi^-K^+K^-$ $\pi^+\pi^-p\bar{p}$
$\pi^+\pi^-\psi; \; \psi\to \begin{cases} \pi^+\pi^-\pi^+\pi^-\pi^0 \\ \pi^+\pi^-\pi^+\pi^- \end{cases}$	360 ± 60	0.074	$(1.45 \pm 0.35)\%$	$\pi^+\pi^-\pi^+\pi^-\pi^+\pi^-$
$\mu^+\mu^-$	2454	0.56	$(2.0 \pm 0.3)\%$ [a]	$\pi^+\pi^-$ K^+K^-

[a] Includes resonance and QED contributions.

TABLE III. $\chi(3415)$ branching ratios.

Decay mode	Events	Efficiency	$B(\psi' \to \gamma\chi)\, B(\chi \to f)$	$B(\chi \to f)$ [a]
$\pi^+\pi^-$	32 ± 6	0.19	$(7.5 \pm 2.1) \times 10^{-4}$	$(1.0 \pm 0.3) \times 10^{-2}$
K^+K^-	27 ± 5.5	0.16	$(7.8 \pm 2.3) \times 10^{-4}$	$(1.0 \pm 0.3) \times 10^{-2}$
$\pi^+\pi^-\pi^+\pi^-$	181 ± 16	0.19	$(3.5 \pm 0.7) \times 10^{-3}$	$(4.6 \pm 0.9) \times 10^{-2}$
$\pi^+\pi^-K^+K^-$	83 ± 11	0.11	$(2.8 \pm 0.7) \times 10^{-3}$	$(3.7 \pm 0.9) \times 10^{-2}$
$\pi^+\pi^-p\bar{p}$	23 ± 6	0.18	$(4.7 \pm 1.3) \times 10^{-4}$	$(0.6 \pm 0.2) \times 10^{-2}$
$\pi^+\pi^-\pi^+\pi^-\pi^+\pi^-$	37 ± 8	0.08	$(1.4 \pm 0.5) \times 10^{-3}$	$(1.9 \pm 0.7) \times 10^{-2}$
$\psi\gamma$	1 ± 1	0.0011	$(2 \pm 2) \times 10^{-3}$	$(3 \pm 3) \times 10^{-2}$

[a] We use $B(\psi' \to \gamma\chi) = 0.075$ as obtained in Sec. III A. The errors quoted for $B(\chi \to f)$ do not include the overall scale uncertainty of 35% due to the error (± 0.0026) in $B(\psi' \to \gamma\chi)$.

the histograms of Figs. 10 and 11 were fit with the superposition of a smoothly varying background term plus the contributions of the various peaks from both χ and ψ' decay into the particular final states. The shapes of these peaks were taken as sums of several Gaussians of different widths corresponding to the range of calculated resolutions. To take account of slightly different systematics in the various decay modes, the χ masses and the overall scales of the resolution widths were allowed to vary along with the relative populations. The results of the mass fits have been incorporated into the best mass values for the three χ states given in the previous section. The populations obtained in these fits are given in Tables III, IV, V, and VI.

Efficiencies for both the ψ' modes used in the normalization and the χ modes were calculated by Monte Carlo methods. Besides the geometrical efficiencies, other significant contributions include the following:

(i) $\pi^+\pi^-K^+K^-$, $\pi^+\pi^-p\bar{p}$—inefficiencies in the time-of-flight selection;

(ii) $\pi^+\pi^-K^+K^-$, K^+K^-—K decay in flight losses;

(iii) $\pi^+\pi^-$, K^+K^-—losses due to cuts used for background removal;

(iv) four-prong, six-prong χ modes—losses due to $\psi' \to \pi^+\pi^-\psi$ elimination cuts.

The resulting efficiencies and branching-ratio products are given in Tables III, IV, and V.

We have estimated χ branching ratios $B(\chi \to f)$

by dividing the branching-ratio products $B(\psi' \to \gamma\chi,\ \chi \to f)$ by the ψ' branching ratios into the χ states $B(\psi' \to \gamma\chi)$. For the $\chi(3415)$ we have used our measurement $B(\psi' \to \gamma\chi(3415)) = 0.075 \pm 0.026$ discussed in Sec. III A above. For the $\chi(3505)$ and $\chi(3550)$ we have used the results given by the SPEAR SP-27 collaboration.[12] The corresponding χ branching ratios are given in the last columns of Tables III, IV, and V. The errors quoted for these branching ratios do not include the overall scale errors due to the uncertainties in the values of $B(\psi' \to \gamma\chi)$ which amount to about 30%.

For completeness we have also exhibited in Table VI the direct branching ratios $B(\psi' \to f)$.[22] These are all about a factor of 5–10 smaller than the corresponding ψ branching ratios. This is roughly the same suppression as for the dilepton branching ratios in ψ and ψ' decay.

c. Search for χ decays into known resonances. The effective mass spectra for numerous combinations of pions and kaons have been examined in an attempt to search for the presence of known resonances. The only significant structure observed comes from ρ and $K^*(891)$ in the 4π and $\pi^+\pi^-K^+K^-$ final states, respectively. The $\pi^+\pi^-$ and $K^\pm\pi^\mp$ effective mass spectra for the $\chi(3415)$ are shown in Fig. 12. All three χ states exhibit substantial ρ and K^* production. The fractions of 4π and $\pi^+\pi^-K^+K^-$ final states which go via $\rho\pi\pi$ and $K^*K\pi$ are summarized in Table VII. It is worth noting that no significant $\rho\rho$ or $K^*(891)$

TABLE IV. $\chi(3505)$ branching ratios.

Decay mode	Events	Efficiency	$B(\psi' \to \gamma\chi)\, B(\chi \to f)$	$B(\chi \to f)$ [a]
$\pi^+\pi^-\pi^+\pi^-$	74 ± 12	0.20	$(1.4 \pm 0.4) \times 10^{-3}$	$(2.0 \pm 0.6) \times 10^{-2}$
$\pi^+\pi^-K^+K^-$	24 ± 7	0.11	$(0.8 \pm 0.3) \times 10^{-3}$	$(1.1 \pm 0.4) \times 10^{-2}$
$\pi^+\pi^-p\bar{p}$	6 ± 4	0.19	$(1.2 \pm 0.8) \times 10^{-4}$	$(1.7 \pm 1.1) \times 10^{-3}$
$\pi^+\pi^-\pi^+\pi^-\pi^+\pi^-$	48 ± 15	0.08	$(1.9 \pm 0.7) \times 10^{-3}$	$(2.7 \pm 1.1) \times 10^{-2}$
$\psi\gamma$	12 ± 4	0.0011	$(2.4 \pm 0.8) \times 10^{-2}$	$(34 \pm 11) \times 10^{-2}$

[a] We use $B(\psi' \to \gamma\chi) = 0.071$ from Ref. 10. The errors quoted for $B(\chi \to f)$ do not include the overall scale uncertainty of 27% due to the error (± 0.019) in $B(\psi' \to \gamma\chi)$.

TABLE V. χ(3550) branching ratios.

Decay mode	Events	Efficiency	$B(\psi' \to \gamma\chi) \, B(\chi \to f)$	$B(\chi \to f)$ [a]
$\pi^+\pi^-$ or K^+K^-	9 ± 4	0.18	$(1.9 \pm 0.8) \times 10^{-4}$	$(2.7 \pm 1.1) \times 10^{-3}$
$\pi^+\pi^-\pi^+\pi^-$	89 ± 12	0.20	$(1.7 \pm 0.4) \times 10^{-3}$	$(2.4 \pm 0.6) \times 10^{-2}$
$\pi^+\pi^-K^+K^-$	47 ± 8	0.12	$(1.5 \pm 0.4) \times 10^{-3}$	$(2.1 \pm 0.6) \times 10^{-2}$
$\pi^+\pi^-p\bar{p}$	13 ± 5	0.19	$(2.6 \pm 1.0) \times 10^{-4}$	$(3.7 \pm 1.4) \times 10^{-3}$
$\pi^+\pi^-\pi^+\pi^-\pi^+\pi^-$	23 ± 15	0.08	$(0.9 \pm 0.6) \times 10^{-3}$	$(1.3 \pm 0.8) \times 10^{-2}$
$\psi\gamma$	4 ± 2	0.0009	$(1.0 \pm 0.6) \times 10^{-2}$	$(14 \pm 8) \times 10^{-2}$

[a] We use $B(\psi' \to \gamma\chi) = 0.070$ from Ref. 10. The errors quoted for $B(\chi \to f)$ do not include the overall scale uncertainty of 29% due to the error (± 0.020) in $B(\psi' \to \gamma\chi)$.

$\bar{K}^*(891)$ signal is observed for any χ state, although there are no obvious selection rules which forbid these processes; the observed ρ and K^* are almost always accompanied by nonresonant meson pairs.

d. Further properties of the χ hadronic decays.

(1) The observed multipion χ decay modes have even G parity. Their branching ratios into such modes are $\gtrsim 1\%$, large enough to suggest that they represent isospin-conserving processes. It follows that the isospin of all the observed χ 's is even. The direct ψ' decay mode,

$$\psi' \to \pi^+\pi^-\pi^+\pi^- ,$$

has a much smaller branching ratio compatible with the known odd G parity of the ψ' and the expected rate on the basis of second-order electromagnetic decay. For the χ (3415), the even isospin coupled with the significant K^+K^- decay mode establishes $I = 0$ as expected on the basis of the $c\bar{c}$ model. The same isospin assignment follows for all the χ states from the usual $|\Delta I| = 0, \pm 1$ selection rule of electromagnetic decay and the zero isospin of the ψ'.

TABLE VI. $\psi'(3684)$ branching ratios into all charged hadrons.

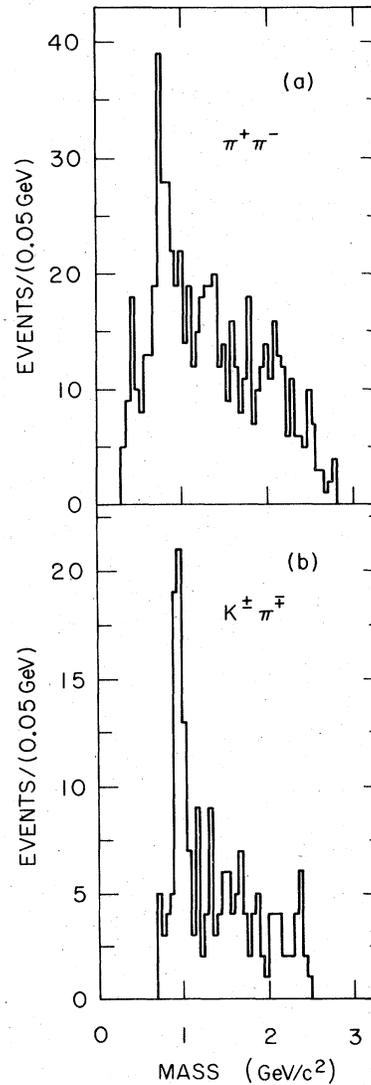| Decay mode	Events	Efficiency	$B(\psi' \to f)$ [a]
$\pi^+\pi^-\pi^+\pi^-$	49 ± 9	0.20	$(0.45 \pm 0.1) \times 10^{-3}$
$\pi^+\pi^-K^+K^-$	53 ± 8	0.12	$(0.8 \pm 0.2) \times 10^{-3}$ to $(1.6 \pm 0.4) \times 10^{-3}$
$\pi^+\pi^-p\bar{p}$	41 ± 7	0.19	$(0.4 \pm 0.1) \times 10^{-3}$ to $(0.8 \pm 0.2) \times 10^{-3}$
$\pi^+\pi^-\pi^+\pi^-\pi^+\pi^-$	9 ± 5	0.08	$(0.15 \pm 0.1) \times 10^{-3}$

[a] See Ref. 22.

FIG. 12. (a) $\pi^+\pi^-$ mass spectrum from χ (3415) $\to \pi^+\pi^-\pi^+\pi^-$ (four combinations per event); (b) $K^\pm\pi^\mp$ mass spectrum from χ(3415) $\to \pi^+\pi^-K^+K^-$ (two combinations per event.

TABLE VII. ρ and $K*$ in χ-state decays.

State	$\dfrac{B(\chi \to \rho^0 \pi^+ \pi^-)}{B(\chi \to \text{all } \pi^+\pi^-\pi^+\pi^-)}$	$\dfrac{B(\chi \to K*^0 K^\pm \pi^\mp)}{B(\chi \to \text{all } \pi^+\pi^- K^+ K^-)}$	$\dfrac{B(\chi \to \rho^0 \pi^+ \pi^-)}{B(\chi \to K*^0 K^\pm \pi^\mp)}$
χ(3415)	0.39 ± 0.12	0.41 ± 0.10	1.2 ± 0.5
χ(3505)	0.24 ± 0.20	0.35 ± 0.18	1.2 ± 1.2
χ(3550)	0.31 ± 0.17	0.25 ± 0.13	1.4 ± 1.1
ψ'(3684)	0.93 ± 0.26	0.42 ± 0.12	1.2 ± 0.6

(2) The observed equality of $\pi^+\pi^-$ and K^+K^- branching ratios agrees with expectations for an SU(3)-singlet assignment for the χ(3415).

(3) The observed ratios of

$$\frac{\chi \to \rho\pi^+\pi^- \to \pi^+\pi^-\pi^+\pi^-}{\chi \to K*K\pi \to K^+\pi^-K^-\pi^+}$$

decay rates are, for all three χ states, in agreement with the SU(3)-singlet predictions of $\frac{3}{2}$ within the rather large estimated errors (see Table VII).[30]

(4) The branching ratios for χ(3415) to $\pi^+\pi^-$, $\pi^+\pi^-\pi^+\pi^-$, and $\pi^+\pi^-\pi^+\pi^-\pi^+\pi^-$, namely, 1%, 4.6%, and 1.9%, are very similar to the values 1.3%, 4.0%, and 2.9% observed for ψ decay to the corresponding modes $\rho\pi$, $\pi^+\pi^-\pi^+\pi^-\pi^0$, $\pi^+\pi^-\pi^+\pi^-\pi^+\pi^-\pi^0$. In making this comparison, a π^0 has been added to go from χ modes to corresponding ψ modes to take account of the opposite G parities.

(5) The radiative decay modes $\chi \to \psi\gamma$ are prominent for both χ(3505) and χ(3550), amounting to roughly 34% and 14%, respectively, of all decays of these states. These branching ratios are far larger than those for any one of the detected hadronic modes. This strong preference for decay into ψ is reminiscent of the behavior of the ψ', about half of whose decays go to ψ.[17] The χ(3415) has only a very small branching ratio for decay to ψ.

IV. SPIN DETERMINATION

A. Information from hadronic decays

For the hadronic modes, one can measure the distribution of θ, the angle between the beam direction and the outgoing photon. The general form is[23-25]

$$W(\cos\theta) = 1 + A\cos^2\theta , \qquad (11)$$

where $|A| \leq 1$.

The value of A can be unambiguously predicted only for spin $J=0$, namely, $A=1$. For spins 1 and 2, there can be several multipoles in the amplitude and the predictions are not unique. However, if one assumes that only the dipole amplitude contributes significantly, one obtains

$$A = -\frac{1}{3}, \quad J = 1 ,$$

$$A = \frac{1}{13} , \quad J = 2 .$$

The actual experimental results, based on using all the observed hadronic decay modes are as follows:

χ(3415) $A = 1.4 \pm 0.4$,

χ(3505) $A = 0.1 \pm 0.4$,

χ(3550) $A = 0.3 \pm 0.4$.

Figure 13(b) and Fig. 14 show the distributions of $|\cos\theta|$ from which the above values of A are
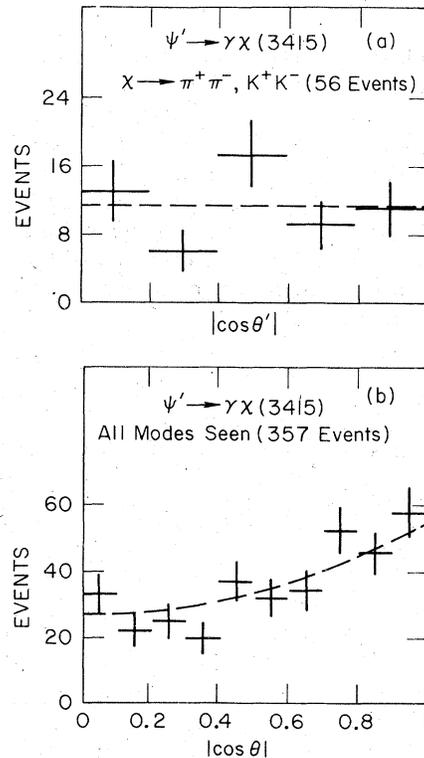

FIG. 13. Decay angular distributions for χ(3415). Angles are defined in text and dashed lines represent the predictions for $J=0$.
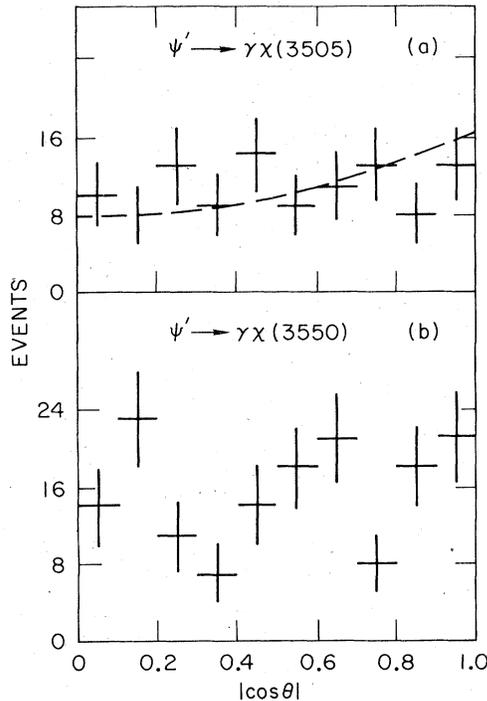
FIG. 14. Angular distributions for (a) $\chi(3505)$ and (b) $\chi(3550)$. The dashed line represents the predictions for $J=0$.

1. Data sample

The data sample of 21 events in Sec. III B is insufficient for a determination of the spin of χ states. This sample is small primarily because we require the conversion of a photon and detection of the conversion pair. We can obtain a larger sample by detecting the photons directly in the shower counters, at the cost of inferior mass resolution, as we have done in our earlier paper.[9]

The lepton pairs from ψ decay are first selected and analyzed in the manner of Sec. III B. In addition, we require the detection of exactly two photons. The azimuthal angles of the photons are determined crudely by using the 24 shower counters as a hodoscope. The polar angles are determined by measuring the longitudinal position of the interaction in the shower counter from the relative pulse heights in the phototubes at either end. The rms angular resolutions are 75 mrad in azimuth and 112 mrad in polar angle. The photon energy information provided by the shower counters is too imprecise to be of use.

The largest background is the decay $\psi' \to \psi\pi^0\pi^0$ where only two of the four photons from π^0 decay are detected. The signal events are twice over-constrained so that most background can be eliminated by doing a 2C fit to the hypothesis $\psi' \to \psi\gamma\gamma$ and making a χ^2 cut ($\chi^2/\text{d.o.f.} < 2$). $\psi' \to \psi\eta$, $\eta \to \gamma\gamma$ events are eliminated by removing all events for which the missing mass recoiling agains the reconstructed ψ is greater than 520 MeV/c^2.

Having performed the 2C fit, we reconstruct the two possible masses of the intermediate state. Figure 15 is an event histogram where each event is plotted twice, once for each solution. The $\chi(3505)$ predominates in cascade decays in agreement with the results from the totally independent event sample discussed in Sec. III B. The observed rms mass width due to resolution of 35 MeV/c^2 agrees with that predicted by Monte Carlo techniques, also shown in the figure as the solid curve. Because of the poor mass resolution, the $\chi(3455)$ and $\chi(3550)$ are not well separated from the $\chi(3505)$. The solid curve includes the contribution from $\psi' \to \psi\pi^0\pi^0$ background, shown separately as the dotted curve.

To reduce background, we consider only events in the mass range 3465 MeV$< M(\chi) <$ 3535 MeV. We have a final sample of 136 events with an estimated background of less than 15% from $\psi' \to \psi\pi^0\pi^0$ decays and events from other χ states. The background is difficult to estimate due to large uncertainties in photon detection efficiency, especially in the range 100 MeV—200 MeV, where the detection efficiency is a rapidly varying function of energy.

derived. Figure 13(a), which applies only to the $\chi(3415) \to \pi^+\pi^-$ or K^+K^- mode, shows the distribution of $|\cos\theta'|$, where θ' is the angle between the dimeson line and the photon. This distribution is expected to be isotropic for $J=0$, and would normally contain terms in $\cos^2\theta'$ and $\cos^4\theta'$ if $J=2$ (the next-lowest allowed spin for a C-even state with a $\pi^+\pi^-$ or K^+K^- decay mode). Unfortunately, the statistics are small, but there is no obvious deviation from isotropy.

The main conclusion from these results is that only the $\chi(3415)$ gives a good fit to spin 0, although spin 2 cannot be rigorously ruled out. The $\chi(3550)$ cannot have spin 1, due to the presence of the $\pi^+\pi^-$ and/or K^+K^- decay modes, and does not fit spin 0 by about 2 standard deviations. The $\chi(3505)$ does not fit spin 0 by greater than 2 standard deviations.

B. The spin of the $\chi(3505)$ from angular correlations

In the decay sequence $\psi' \to \chi\gamma$, $\chi \to \psi\gamma$, $\psi \to l^+l^-$, the angular distributions of the photons and leptons with respect to the beam direction and to each other depend on the spin of the χ state.[23-25] These distributions can then, in principle, be used to determine the χ spin.
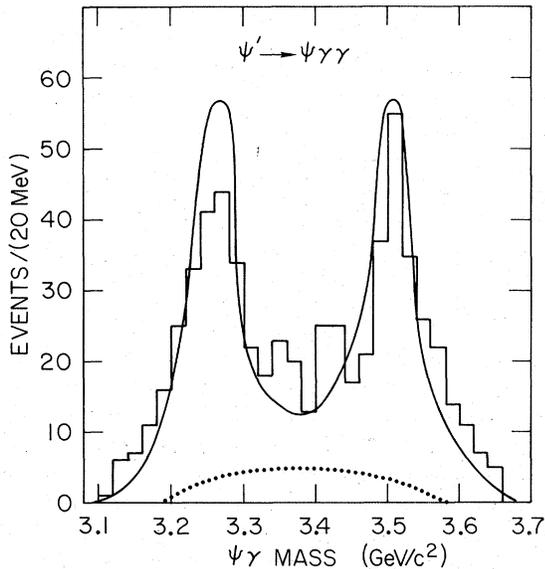
FIG. 15. The reconstructed mass of $\chi\gamma$ pairs fit to $\psi' \rightarrow \psi\gamma\gamma$ for events where both photons are detected in the shower counters. The smooth curves are explained in the text.

2. Spin determination of $\chi(3505)$

Angular distributions have been calculated by several theorists.[23-25] We use the method of Karl, Meshkov, and Rosner.[23] We define the following four independent momentum-energy four-vectors:

e_1: the positron beam (in the laboratory frame);

γ_1: the photon from ψ' decay (in the laboratory frame);

γ_2: the photon from χ decay (in the χ rest frame);

e_2: the positive lepton from ψ decay (transformed first to the χ rest frame and then to the ψ rest frame).

We define the corresponding unit three-vectors $\hat{e}_1$, $\hat{\gamma}_1$, $\hat{\gamma}_2$, and $\hat{e}_2$ as the normalized spatial parts of the above four-vectors. The angular distributions can be expressed in terms of five independent parameters defined as follows:

$$\cos\alpha = \hat{\gamma}_1 \cdot \hat{\gamma}_2 \quad (-1 \le \cos\alpha \le 1),$$

$$\cos\theta_1 = \hat{e}_1 \cdot \hat{\gamma}_1 \quad (-1 \le \cos\theta_1 \le 1),$$

$$\cos\theta_2 = \hat{e}_2 \cdot \hat{\gamma}_2 \quad (-1 \le \cos\theta_2 \le 1),$$

$\phi_1 \ (-\pi \le \phi_1 \le \pi)$ ϕ_1 is the azimuthal angle of $\hat{e}_1$ in the coordinate system, where $\hat{\gamma}_1$ defines the z axis and $\hat{\gamma}_2$ defines $\phi = 0$,

$\phi_2 \ (-\pi \le \phi_2 \le \pi)$ ϕ_2 is the azimuthal angle of $\hat{e}_2$ in the coordinate system, where $\hat{\gamma}_2$ defines the z axis and $\hat{\gamma}_1$ defines $\phi = 0$.

The parameters are chosen such that a phase-space distribution corresponds to a uniform density in the five-dimensional space, except for experimental detection biases. In addition, if all four processes ($e^+e^- \rightarrow \psi'$, $\psi' \rightarrow \chi\gamma$, $\chi \rightarrow \psi\gamma$, $\psi \rightarrow l^+l^-$) conserve parity, the angular distribution is separately invariant under the four independent transformations $\hat{e}_1 \rightarrow -\hat{e}_1$, $\hat{\gamma}_1 \rightarrow -\hat{\gamma}_1$, $\hat{\gamma}_2 \rightarrow -\hat{\gamma}_2$, and $\hat{e}_2 \rightarrow -\hat{e}_2$. Assuming parity conservation, we can use these transformations on an event-by-event basis to restrict the range of any four out of the five parameters to non-negative values: We choose to apply these transformations to each event to force all parameters except ϕ_2 to be non-negative. This reduces our volume in the five-dimensional space sixteenfold.

If the χ state has spin 0, the predicted distribution is unique, as both radiative decays must be pure dipole. If the χ state has spin 1, the amplitude for each transition can be an arbitrary superposition of dipole and quadrupole amplitudes. Hence, the distribution depends on two free parameters, the ratio of the quadrupole-to-dipole amplitude in each decay. If χ has spin 2, octupole transitions can also contribute, and the distributions depend on four free parameters.

Our method for attempting to determine the spin is a maximum-likelihood fit to the three hypotheses that the χ has spin 0, 1, or 2. We use the full angular distribution in all five angular parameters. We bin the data in equal size bins, using three bins in each parameter except for ϕ_2, which we divide into six bins, making a total of 486 bins in the five-dimensional space. The bin sizes are chosen to be large compared to experimental resolution, thereby minimizing systematic errors. The binned data are corrected for detection efficiency determined by a Monte Carlo simulation of the apparatus. The detection efficiency is computed and corrected separately for $\psi \rightarrow e^+e^-$ and $\psi \rightarrow \mu^+\mu^-$ events. The relative number of corrected events in each bin should be proportional to the theoretically predicted distribution integrated over the bin.

As mentioned above, the distribution for χ spin 0 is unique, while for χ spin 1 (2) the distribution depends on two (four) free parameters. We assume that for χ spin 2 the octupole transition amplitude is negligible for both ψ' and χ decay, reducing the number of free parameters from four to two. The results of the maximum-likelihood analysis over the full five-dimensional angular distribution will be given below. We first show the most important projection.

Figure 16 is a plot of the corrected data as a function of $\cos\theta_2$. The curves are the predicted distributions for various χ spin hypotheses, as-
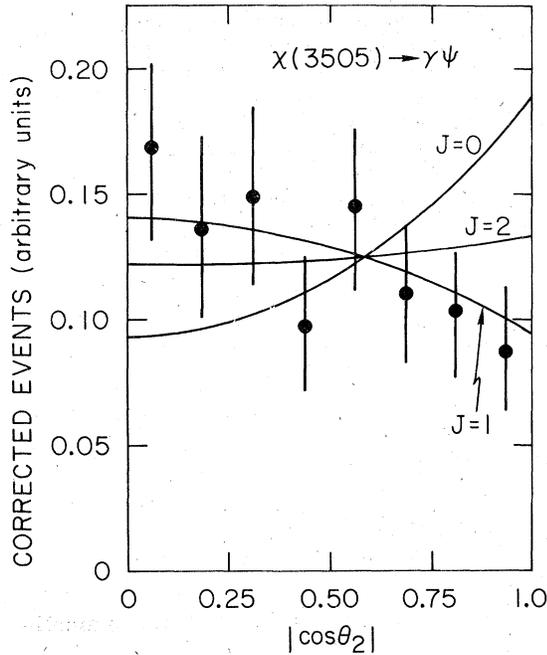
FIG. 16. Cosine of the angle between the photon direction and the lepton direction in $\chi \to \gamma\psi$; $\psi \to l^+l^-$. The data have been corrected for acceptance biases. The solid curves represent predicted curves for a given χ spin, assuming pure dipole decay.
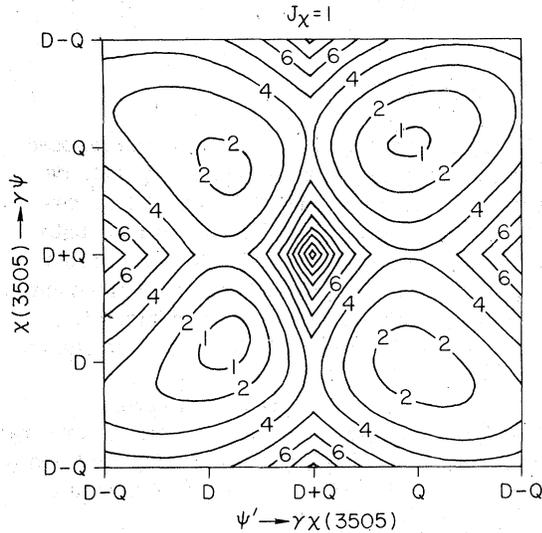

FIG. 17. Likelihood function assuming $J_\chi = 1$ as a function of the relative dipole and quadrupole amplitudes for each decay. The contours are explained in the text. D indicates pure dipole decay, and Q pure quadrupole decay. $D \pm Q$ indicate equal dipole and quadrupole amplitudes with the relative phase indicated. The scale is linear in the square of either amplitude.
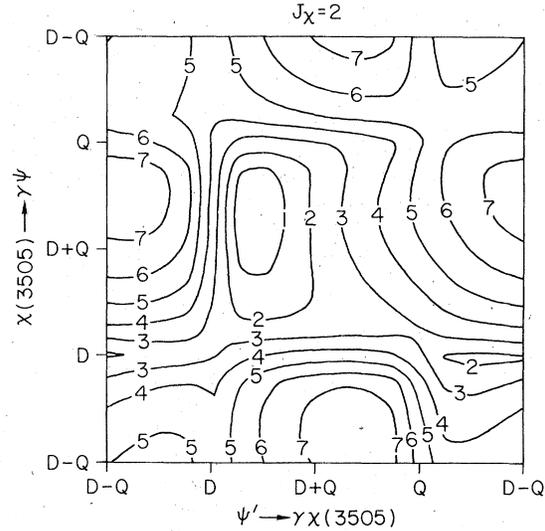

FIG. 18. Likelihood function assuming $J_\chi = 2$ as a function of the relative dipole and quadrupole amplitudes for each decay, assuming the octupole amplitudes are zero. The contours are explained in the text. The scale is the same as that for the preceding figure.

suming pure dipole decay. Spin 0 is disfavored by over 4 standard deviations, while either spin 1 or 2 fit the data reasonably well. In principle, the distribution in $\cos\theta_1$ is just as sensitive to the χ spin as the distribution in $\cos\theta_2$, but the geometry of the detector is such that photons within about 45 degrees of the beam are not detected, thereby washing out most of the sensitivity.

The results of the full five-dimensional fit are plotted in Fig. 17 and Fig. 18 (see also Tables VIII and IX). The figures show the separate relative likelihood function for spin 1 and spin 2 as a function of the relative dipole and quadrupole amplitudes for each decay. Contours are plotted at integral intervals in standard deviation assuming the likelihood function is a Gaussian; that is at n standard deviations the likelihood function is $\exp(-n^2/2)$ times maximum. The likelihood function for spin 1 has four local maxima, while for

TABLE VIII. Relative likelihood functions as a function of $\chi(3505)$ spin, assuming $\psi' \to \gamma\chi$ and $\chi \to \gamma\psi$ are both pure dipole transitions.

$\chi(3505)$ spin	Relative likelihood	Standard deviations
1	1.00	0.0
2	0.063	2.3
0	2.85×10^{-5}	4.6

TABLE IX. Relative likelihood functions as a function of $\chi(3505)$ spin, allowing both decays to be arbitrary superpositions of normalized real dipole and quadrupole amplitudes. Relative likelihood functions are given at all six local maxima of the likelihood function, as well as for spin 0, where both decays must uniquely be pure dipole. (The spin-0 likelihood function is corrected for the fact that there are two fewer free parameters than for spin 1 or 2.) Also listed for each local maximum is the square of the quadrupole amplitude for each decay, with the sign being the relative phase between dipole and quadrupole amplitudes. Errors are given for the best solution for each spin. The amplitudes are normalized such that $D^2 + Q^2 = 1$, where D and Q are the dipole and quadrupole amplitudes, respectively.

$\chi(3505)$ spin	Signed square of quadrupole amplitude		Relative likelihood	Standard deviations
	$\psi' \to \gamma\chi$	$\chi \to \gamma\psi$		
1	$+0.09 \pm 0.11$	$+0.09 \pm 0.12$	0.33	1.5
1	$+0.09$	$+0.90$	0.08	2.2
1	$+0.98$	-0.02	0.13	2.0
1	$+0.97$	-0.98	0.25	1.7
2	$+0.18^{+0.16}_{-0.07}$	$+0.73^{+0.15}_{-0.36}$	1.00	0.0
2	-0.72	$+0.00$	0.24	1.7
0	$\circ\circ\circ$	$\circ\bullet\bullet$	1.87×10^{-5}	4.7

spin 2 it has two local maxima. Table IX lists the six local maxima, as well as the unique solution for spin 0 and gives the relative likelihood of each solution. Spin 0 is ruled out at the level of almost 5 standard deviations. We cannot, however, distinguish between spin 1 and spin 2. Allowing all possible combinations of dipole and quadrupole amplitudes spin 2 is favored over spin by 1.5 standard deviations. If we assume that both transitions are pure dipole, spin 1 is favored over spin 2, but by only 2.3 standard deviations. We note that for spin 1, one of the local maxima corresponds to both decays being nearly pure dipole, while the other maxima correspond to one or both decays being nearly pure quadrupole. On theorectial grounds, it is unlikely that either decay would be nearly pure quadrupole. For χ spin 2 neither solution is closed to the dipole-dipole point.

The results given do not take systematic errors into account. The only large systematic error comes from contamination from $\psi' \to \psi\pi^0\pi^0$ and from cascade decays of other χ states. We can estimate this error by varying the width of the χ mass cut, thereby changing the background-to-signal ratio substantially. In all cases, from narrowing the mass cut by 30% to removing it entirely, the likelihood-function maxima move by less than 1 standard deviation.

For χ spin 1, the multipole amplitudes (dipole $= D$, quadrupole $= Q$) are related to pure helicity amplitudes in a very simple way.[23] For each of the separate decays $\psi' \to \gamma\chi$ and $\chi \to \gamma\psi$, the χ has three possible helicity states, $h = 0$ and $h = \pm 1$. If parity is conserved, the decay amplitudes of $h = -1$ and $h = +1$ must be equal, so there are only two independent helicity amplitudes which we call h_0 and

h_1. The helicity amplitudes and multipole amplitudes are related as follows:

$$h_0 = \frac{1}{\sqrt{2}} (D + Q),$$

$$h_1 = \frac{1}{\sqrt{2}} (D - Q),$$

or conversely:

$$D = \frac{1}{\sqrt{2}} (h_0 + h_1),$$

$$Q = \frac{1}{\sqrt{2}} (h_0 - h_1).$$

Hence, in Fig. 17, $D + Q$ and $D - Q$ correspond to pure helicity zero and pure helicity one, respectively. Note that pure helicity states, especially $h = 0$, are strongly disfavored for both decays. For χ spin 2, the pure helicity states $h = 0$, $h = 1$, and $h = 2$ involve octupole components, and thus do not appear anywhere in Fig. 18.

We thus can draw the following conclusions from this analysis.

1. The $\chi(3505)$ cannot have spin zero.

2. If the $\chi(3505)$ has spin 1, each of the two transitions is nearly pure dipole or nearly pure quadrupole. Neither transition occurs with pure χ helicity zero or one.

3. If the $\chi(3505)$ has spin 2, the preferred solutions (assuming no octupole contributions) are the specific linear combinations of dipole and quadrupole amplitudes given in Table IX.

4. Even if we restrict both decays to be pure dipole, which is a preferred solution for spin 1 but not for spin 2, spin 1 is favored by only 2.3 stand-

TABLE X. Summary of χ spin-parity information.

State and mass (Information source)	$\pi^+\pi^-/K^+K^-$ final state	Photon angular distribution in hadronic decays	Cascade angular correlations	Suggested J^P
$\chi(3415)$ 3414 ± 3 MeV	$J^P = 0^+,\ 2^+,\dots$	Consistent with $J=0$	$\cdots$	0^+
$\chi(3505)$ 3503 ± 4 MeV	$J^P \neq 0^+,\ 2^+,\dots$ suggested	$J \neq 0$ (2σ level)	$J \neq 0$ (5σ level)	1^+
$\chi(3550)$ 3551 ± 4 MeV	$J^P = 0^+,\ 2^+,\dots$	$J \neq 0$ (2σ level)	$\cdots$	2^+
$\chi(3455)$ 3454 ± 7 MeV		No information		

ard deviations. Hence, even under that restriction spin 2 cannot be ruled out.

C. Summary of the spin information

We summarize the totality of the available information on spins for the χ states in Table X. Obviously, the data are inadequate to provide an unambigous set of spin assignments irrespective of models. However, if we assume that the three main states are the expected $^3P_0$, $^3P_1$, and $^3P_2$ bound states of a quark and an antiquark, there is a unique spin assignment which is given in the last column of Table X. Some additional support for these choices comes from the following considerations:

(a) None of the three well-established states can be a pseudoscalar. This is of some significance since the pseudoscalar states are the only predicted states which have not been identified.

(b) On the basis of simple bound-state models for the $c\bar{c}$ systems decaying via an electric dipole transition, one expects that the widths $\Gamma(\psi' \to \chi\gamma)$ for each state are proportional to $(2J+1)k_\gamma{}^3$, where J is the χ spin and k_γ is the photon energy. From the results of the SPEAR SP-27 collaboration,[12] these three widths are within about 30% of each other. This result is compatible with the above $(2J+1)k_\gamma{}^3$ factor only for the choice of spins given in Table X.

There is no information on the spin of the $\chi(3455)$.

V. DISCUSSION AND CONCLUSIONS

From the analysis which has been presented in this paper we can arrive at the following conclusions:

1. There are three clearly established states at masses 3414 ± 3, 3503 ± 4, and 3551 ± 4 MeV/c^2

produced in radiative decays of the ψ'. The errors quoted do not include an overall mass-scale uncertainty of ±4 MeV/c^2. Each of these states has been observed in this experiment in at least two independent ways, and all have also been observed in other experiments. The observed widths of the states are in all cases consistent with the experimental resolutions, setting upper limits for the decay full widths of about 20 MeV.

2. All of the above states have significant hadronic decay modes. The data on these decays are all consistent with isospin-zero, SU(3)-singlet behavior as expected for $c\bar{c}$ bound states.

3. Both the $\chi(3505)$ and $\chi(3550)$ exhibit significant branching ratios for radiative decays to ψ. From theoretical estimates based on electric dipole transitions,[26][27] one might expect the partial widths for these decays to be of the order of a few hundred keV. From the branching ratios, one would then estimate full widths for these χ states which are of the order of a few MeV or less. The $\chi(3415)$ radiative branching ratio is very small. If its radiative width is comparable to that of the other two states, its full width is substantially larger.

4. None of the above three states can be a pseudoscalar. Unique spin-parity assignments cannot be made, but if one assumes that they are the expected $^3P_0$, $^3P_1$, and $^3P_2$ $c\bar{c}$ states, a highly preferred assignment is possible. Specifically, the $\chi(3415)$, $\chi(3505)$, and $\chi(3550)$ are assigned to $J^P = 0^+, 1^+, 2^+$. It is interesting to note that if this assignment is correct, the $\chi(3505)$ is the charmonium analog of the long-studied A_1.

5. All transitions on which angular distribution data exist, namely, $\psi' \to \gamma\chi(3415)$, $\gamma\chi(3505)$, $\gamma\chi(3550)$ and $\chi(3505) \to \gamma\psi$ are consistent with dominance by the electric dipole amplitude.

6. In the $\gamma\psi$ decay mode, there is some evidence for another χ state at a mass of 3455 ± 10 or perhaps 3340 ± 10 MeV. There is no evidence for hadronic decay modes of this state. A possible interpretation might be the η'_c, the pseudoscalar expected to lie below the ψ', although the ψ'-η'_c mass splitting would, in this interpretation, appear to be surprisingly large. This interpretation leads to the other theoretical problems as well.[28] Another possibility is that the $\chi(3455)$ is the lowest-lying $^1D_2$ state of charmonium.[29]

7. The DASP group has reported evidence for a state at 2830 MeV produced radiatively from the ψ and decaying into two photons.[13] Although the

mass separation from the ψ is again unexpectedly large, this state may be a candidate for the pseudoscalar η_c. Our study of the inclusive photon spectrum from the ψ sets a 90% confidence level upper limit of 3.9% for the total $\psi \to \gamma X(2830)$ branching ratio. Furthermore, we also set an upper limit for the $\psi' \to \gamma X(2830)$ of 1%.

*Present address: DESY, Hamburg, Germany.

†Present address: Laboratori Nazionali di Frascati dell'INFN, Rome, Italy.

‡Present address: CERN, Geneva, Switzerland.

§Present address: Massachusetts General Hospital, Boston, Massachusetts.

‖Present address: LPNHE, Universite Paris VI, Paris, France.

¶Present address: Centre d'Etudes Nucleaires de Saclay, France.

[1]T. Appelquist and H. D. Politzer, Phys. Rev. Lett. 34, 46 (1975); T. Appelquist et al., ibid. 34, 365 (1975).

[2]M. K. Gaillard, B. W. Lee, and J. L. Rosner, Rev. Mod. Phys. 47, 277 (1975).

[3]C. G. Callan et al., Phys. Rev. Lett. 34, 52 (1975).

[4]E. Eichten et al., Phys. Rev. Lett. 34, 369 (1975).

[5]A. M. Boyarski et al., Phys. Rev. Lett. 34, 1357 (1975).

[6]V. Lüth et al., Phys. Rev. Lett. 35, 1124 (1975).

[7]W. Braunschweig et al., Phys. Lett. 57B, 407 (1975).

[8]G. J. Feldman et al., Phys. Rev. Lett. 35, 821 (1975).

[9]W. Tanenbaum et al., Phys. Rev. Lett. 35, 1323 (1975).

[10]J. S. Whitaker et al., Phys. Rev. Lett. 37, 1596 (1976).

[11]H. Rieseberg, invited talk on results from the DESY-Heidelberg Collaboration , in Particle Searches and Discoveries—1976, proceedings of the Second International Conference in High Energy Physics at Vanderbilt University, edited by R. S. Panvini (AIP, New York, 1976), p. 274.

[12]C. J. Biddick et al., Phys. Rev. Lett. 38, 1324 (1977).

[13]W. Braunschweig et al., Phys. Lett. 67B, 243 (1977).

[14]J. S. Whitaker, LBL Report No. LBL-5518 (Ph. D. thesis) (unpublished) contains more detailed information on many of the topics covered in this paper.

[15]J.-E. Augustin et al., Phys. Rev. Lett. 34, 233 (1975).

[16]These chambers are discussed in detail in B. Sadoutlet, LBL Report No. LBL-4221, 1975 (unpublished).

[17]G. S. Abrams et al., Phys. Rev. Lett. 34, 1181 (1975).

[18]J. W. Simpson et al., Phys. Rev. Lett. 35, 699 (1975).

[19]The polar-angle cutoff used is $|\cos\theta_\gamma| < 0.65$, rather than 0.6 as in Sec. III A, in order to provide a somewhat larger sample. There is no significant loss of detection efficiency near $|\cos\theta_\gamma| = 0.65$.

[20]W. Tanenbaum et al., Phys. Rev. Lett. 36, 402 (1976).

[21]G. J. Feldman and F. J. Gilman, Phys. Rev. D 12, 2161 (1975).

[22]The ψ' branching ratios have been corrected in order to remove the nonresonant background. For $\psi' \to 4\pi$ and $\psi' \to 6\pi$, which must be second-order electromagnetic decays because of G-parity conservation, the ratio of nonresonant background to resonant ψ' decay must be the same as for $\psi' \to \mu^+\mu^-$, for which the nonresonant background can be calculated by QED. For $\psi' \to \pi\pi KK$ and $\psi' \to \pi\pi p\bar{p}$, which can also proceed by strong decay, the nonresonant background cannot be uniquely determined from our data. The smaller (larger) value for the branching ratio applies if the decay is entirely electromagnetic (strong).

[23]G. Karl, S. Meshkov, and J. L. Rosner, Phys. Rev. D 13, 1203 (1976).

[24]L. S. Brown and R. N. Cahn, Phys. Rev. D 13, 1195 (1976).

[25]P. K. Kabir and A. J. G. Hey, Phys. Rev. D 13, 3161 (1976).

[26]E. Eichten et al., Phys. Rev. Lett. 36, 500 (1976).

[27]J. D. Jackson, Phys. Rev. Lett. 37, 1107 (1976).

[28]M. S. Chanowitz and F. J. Gilman, Phys. Lett. 63B, 178 (1976).

[29]H. Harari, Phys. Lett. 64B, 469 (1976).

[30]A. D. Dolgov and A. Yu. Khodjamirian, Yerevan Physics Institute Report No. EQN-237(30)-77 (unpublished). We wish to thank F. J. Gilman for bringing this paper to our attention.